HHS Public Access

Author manuscript

Oncogene. Author manuscript; available in PMC 2018 December 28.

Published in final edited form as:

Oncogene. 2016 April 14; 35(15): 1909–1918. doi:10.1038/onc.2015.253.

TSH overcomes *Braf*^{V600E}-induced senescence to promote tumor progression via downregulation of p53 expression in papillary thyroid cancer

M Zou[#1], **EY Baitei**[#1], **RA Al-Rijjal**[1], **RS Parhar**[2], **FA Al-Mohanna**[2], **S Kimura**[3], **C Pritchard**[4], **HA Binessa**[1], **AS Alzahrani**[5], **HH Al-Khalaf**[6], **A Hawwari**[1], **M Akhtar**[7], **AM Assiri**[#8], **BF Meyer**[1], and **Y Shi**[1]

[1]Department of Genetics, King Faisal Specialist Hospital and Research Centre, Riyadh, Saudi Arabia

[2]Department of Cell Biology, King Faisal Specialist Hospital and Research Centre, Riyadh, Saudi Arabia

[3]Laboratory of Metabolism, National Cancer Institute, National Institutes of Health, Bethesda, MD, USA

[4]Department of Biochemistry, University of Leicester, Lancaster Road, Leicester, UK

[5]Department of Medicine, King Faisal Specialist Hospital and Research Centre, Riyadh, Saudi Arabia

[6]Department of Molecular Oncology, King Faisal Specialist Hospital and Research Centre, Riyadh, Saudi Arabia

[7]Department of Pathology, King Faisal Specialist Hospital and Research Centre, Riyadh, Saudi Arabia

[8]Department of Comparative Medicine, King Faisal Specialist Hospital and Research Centre, Riyadh, Saudi Arabia

[#] These authors contributed equally to this work.

Abstract

The *BRAF*^{V600E} mutation is found in approximately 40% of papillary thyroid cancers (PTC). Mice with thyroid-specific expression of *Braf*^{V600E} (TPO–*Braf*^{V600E}) develop PTC rapidly with high levels of serum thyroid-stimulating hormone (TSH). It is unclear to what extent the elevated TSH contributes to tumor progression. To investigate the progression of *Braf*^{V600E}-induced PTC (BVE–PTC) under normal TSH, we transplanted BVE–PTC tumors subcutaneously into nude and TPO–*Braf*^{WT} mice. Regression of the transplanted tumors was observed in both nude and TPO–*Braf*^{WT} mice. They were surrounded by heavy lymphocyte infiltration and oncogene-induced senescence (OIS) was demonstrated by strong β-gal staining and absence of Ki-67 expression. In

Correspondence: Dr Y Shi, Departments of Genetics, King Faisal Specialist Hospital and Research Centre, MBC#3, Takhassusi street, PO Box 3354, Riyadh 11211, Saudi Arabia. yufei@kfshrc.edu.sa.

CONFLICT OF INTEREST

The authors declare no conflict of interest.

contrast, BVE–PTC transplants continued to grow when transplanted into TPO–*Braf*^{V600E} mice. The expression of *Trp53* was increased in tumor transplants undergoing OIS. *Trp53* inactivation reversed OIS and enabled tumor transplants to grow in nude mice with characteristic cell morphology of anaplastic thyroid cancer (ATC). PTC-to-ATC transformation was also observed in primary BVE–PTC tumors. ATC cells derived from *Trp53* knockout tumors had increased PI3K/AKT signaling and became resistant to *Braf*^{V600E} inhibitor PLX4720, which could be overcome by combined treatment of PI3K inhibitor LY294002 and PLX4720. In conclusion, BVE–PTC progression could be contained *via* p53-dependent OIS and TSH is a major disruptor of this balance. Simultaneous targeting of both MAPK and PI3K/AKT pathways offer a better therapeutic outcome against ATC. The current study reinforces the importance of rigorous control of serum TSH in PTC patients.

INTRODUCTION

Thyroid cancer is the most common type of endocrine malignancy and its incidence has risen rapidly in recent years, especially among women.[1] Histologically, it can be classified into papillary thyroid cancer (PTC), follicular thyroid cancer and anaplastic thyroid cancer (ATC). PTC accounts for more than 80% of thyroid cancer cases.[2] Surgery combined with radioactive iodine therapy is still the treatment of choice for both PTC and follicular thyroid cancer.[3] However, the 10-year recurrence rate is about 20–30% among patients who are older than 45 years and have large invasive tumors or extensive lymph-node metastases.[4,5] Currently, there is no effective treatment for radioiodine-resistant metastatic disease, with a 10-year survival rate of less than 15%.[6] A better understanding of thyroid cancer biology is necessary to develop new treatment strategies.

The RAS–RAF–MEK–ERK MAP kinase signaling pathway (MAPK) has an important role in the initiation and progression of PTC. Among genetic alterations detected in PTC, *BRAF*^{V600E} is the most common mutation (44%) and has been associated with poorer prognosis and more aggressive clinical outcome.[7] *BRAF*^{V600E} can downregulate the expression of genes (*NIS, TG, TPO*) involved in thyroid hormone synthesis and promote dedifferentiation processes in PTC.[8,9] In humans, serum thyroid-stimulating hormone (TSH) increases with age and mean TSH is significantly higher in thyroid cancer patients.[10] Even though serum TSH is within normal range from 0.4 to 4.0 (mIU/l) in most PTC patients, the frequency of malignancy increases when TSH is greater than 0.9 mU/l.[11–13] In *Braf*^{V600E}-induced PTC mouse models, however, serum TSH is more than 100-fold higher owing to severe hypothyroidism.[14–16] The difference may be due to the fact that, in humans, PTC develops from minority loci of thyrocytes carrying *BRAF*^{V600E} and the surrounding majority of normal thyrocytes can still maintain normal thyroid function, whereas, in mice, all the thyrocytes carry mutant *Braf*^{V600E} and normal thyroid function cannot be maintained, resulting in hypothyroidism with elevated TSH. In mice with normal serum TSH[16] or blocked TSH signaling,[15] tumorigenesis may occur but is significantly delayed, resulting in small and localized tumors. Shimamura *et al.*[17] demonstrated recently that *Braf*^{V600E} cannot induce a tumor when it is expressed postnatally in thyrocytes without TSH stimulation. These studies indicate that development of aggressive BVE–PTC requires constant TSH stimulation.

Braf^{V600E}-induced senescence occurs in human and mouse naevi, protecting melanocytes against *Braf*^{V600E}-driven proliferation and progression into melanoma.[18,19] This process has not been demonstrated in mouse models of *Braf*^{V600E}-induced thyroid cancer and elevated TSH may be involved in preventing oncogene-induced senescence (OIS). It is known that TSH stimulates the growth and development of thyroid cancer and elevated serum TSH is associated with higher thyroid cancer incidence and recurrence.[20–22] The study by Franco *et al.*[15] demonstrated that, once PTC is established, suppression of TSH does not change the phenotype. However, it is not known whether tumors will continue to progress or OIS will occur to suppress tumor progression under normal serum TSH. In the present study, we investigated BVE–PTC progression under normal serum TSH and explored the molecular mechanisms regulating the process.

RESULTS

Regression of BVE–PTC transplants in nude and TPO–*Braf*^{WT} mice To investigate whether tumors can continue to grow under normal TSH, we collected 16 BVE–PTC tumors from 4- to 6-month-old TPO–*Braf*^{V600E} mice and transplanted them subcutaneously into eight nude and eight TPO–*Braf*^{WT} mice, respectively. These tumor transplants were monitored for up to 7 months. As shown in Figure 1A, serum TSH levels from nude and TPO–*Braf*^{WT} mice were more than 100-fold lower than TPO–*Braf*^{V600E} mice. The serum TSH levels from five TPO–*Braf*^{V600E} mice (5 months old) were all above the detection limit of 50 000 pg/ml. The average TSH levels from five TPO–*Braf*^{WT} and five nude mice of the same age were 439.6 ± 39.8 and 426.4 ± 9.6 pg/ml, respectively. The mice were genotyped and a representative result is shown in Figure 1B. Tumor transplants were not able to grow and often regressed by more than 50% over the 7-month period. Large cysts were formed in 2 of the 16 tumor transplants. Histology of tumor transplants showed heavy lymphocyte infiltration surrounding the tumor tissue (Figure 1C). Macrophages were often present in the empty spaces of the tumor tissue, which were more frequently seen in the TPO–*Braf*^{WT} mice (Figure 1C, c and d) than in the nude mice (Figure 1C, a and b), indicating tumor clearance by the macrophages. We next investigated whether BVE–PTC tumor transplants could grow subcutaneously in TPO–*Braf*^{V600E} mice under high serum TSH. As shown in Figure 1D, tumor transplants could continue to grow in TPO–*Braf*^{V600E} mice. The average weight of 4-month-old tumor transplants from TPO–*Braf*^{V600E} mice was 1410 ± 1067 mg as compared with 36.3 ± 11.4 mg from TPO–*Braf*^{WT} mice ($P < 0.01$). The average weight of tumors before transplantation was 76.0 ± 12.6 mg. The histology of the tumor transplants from TPO–*Braf*^{V600E} mice showed significant tumor growth and less lymphocyte infiltration, although macrophages could still be seen in the empty spaces of tumor tissue. Furthermore, the BVE–PTC tumor transplants could continue to grow in TPO–*Braf*^{WT} mice after they developed hypothyroidism following treatment of anti-thyroid drug propylthiouracil (0.1% in drinking water).

Induction of senescence by *Braf*^{V600E} in BVE–PTC transplants via upregulation of *Trp53*

To investigate the mechanisms leading to tumor regression in tumor transplants under normal serum TSH, we studied p53 expression by western blot analysis of primary BVE–PTC tumors and tumor transplants. As shown in Figure 2A, more than fivefold increase in

p53 expression was observed in a BVE–PTC tumor transplant when compared with that from a 2-month-old primary tumor. There was also a gradual increase in p53 expression from primary tumors: lower expression in the early stage of the tumor (2 months old) and higher expression in the late stage of the tumor (4–6 months old). This may represent a compensatory mechanism of p53 against *Braf*^{V600E}-driven tumor progression. No significant change was observed in *Cdkn2a*(p16^{INK4A}) and *Cdkn1a*(p21$^{CIP1/WAF1}$) expression (data not shown). The p53 expression was associated with strong senescence-associated beta-galactosidase (SA-beta-Gal) activity (strong SA-beta-Gal staining) and the absence of cell proliferation (absence of Ki-67 immunostaining) in the tumor transplants, whereas no SA-beta-Gal staining and strong Ki-67 immunostaining were demonstrated in primary BVE–PTC tumors (Figure 2B). These data suggest that *Braf*^{V600E}-induced senescence has a major role in tumor regression and is mediated by p53. Heavy lymphocyte and macrophage infiltration in the tumor transplants indicate that innate immune response may be triggered by OIS for tumor clearance. To investigate what cytokines and chemokines were involved, we analyzed 32 cytokines and chemokines in the fluid of cysts from two tumor transplants and compared with those in the 48-h conditioned culture medium from the BVE–PTC cell line which we established from a 6-month-old primary BVE–PTC tumor. As shown in Figure 2C, the production of inflammatory cytokines and chemokines was significantly increased in the tumor fluid such as MIP-1α (macrophage inflammatory protein-1α, which is involved in the acute inflammatory response for the recruitment and activation of polymorphonuclear leukocytes), MIP-1β (a chemoattractant for natural killer cells and monocytes), interleukin (IL)-1β (produced by activated macrophages), and TNF (tumor necrosis factor, also called TNF-α), which is also involved in the acute inflammatory response and produced mainly by activated macrophages. The significance of elevated IL-10 (an anti-inflammatory cytokine) and eotaxin in the fluid is unclear, but they may have a role in the acute inflammatory response. In contrast, many tumor-promoting cytokines and chemokines were significantly reduced in the tumor fluid, such as VEGF (vascular endothelial growth factor), G-CSF (granulocyte colony-stimulating factor),[23] LIF (leukemia inhibitory factor),[24] IL-13,[25] KC (keratinocyte chemoattractant),[26] and MIP-2 (macrophage inflammatory protein 2), which has a role in carcinogenesis by stimulating engraftment,[27] and MCP-1 (monocyte chemoattractant protein-1) (Figure 2D). The production of MCP-1 by tumors has been shown to be responsible for the recruitment of immunosuppressive macrophages, and neutralization of MCP-1 reduces the growth of prostate, breast and lung cancer in mice.[28] These data suggest that OIS can reduce autocrine production of many tumor-promoting cytokines/chemokines by tumor cells, and enhance autocrine/paracrine production of anti-tumor cytokines/chemokines by both tumor cells and infiltrating lymphocytes.

Inhibition of *Braf*^{V600E}-induced senescence by TSH in BVE–PTC cells via downregulation of p53 expression

To investigate whether TSH can downregulate p53 expression and inhibit *Braf*^{V600E}-induced senescence, we analyzed p53 expression in primary BVE–PTC cell cultures. In the absence of TSH, primary BVE–PTC cells could not replicate and displayed characteristic features of cellular senescence such as enlarged and flattened cell morphology with multiple or enlarged nuclei, a vacuolated cytoplasm and increased SA-beta-Gal staining (Figure 3A). When TSH

was added into the culture, primary BVE–PTC cells gradually replicated into an immortalized cell line with reduced p53 expression, loss of cellular senescence and decreased SA-beta-Gal staining (Figure 3A). During 5 months of continued culture (about 40 passages), the immortalized cell line eventually became TSH-independent and highly tumorigenic when injected into nude or TPO–$Braf^{WT}$ mice: all five nude and TPO–$Braf^{WT}$ mice grew tumors within 6 weeks following subcutaneous injection of 10^6 cells. In a BVE–PTC cell line with 18 passages, p53 expression was downregulated by 1.6-fold upon 72-h incubation with 10mU/ml TSH (Figure 3B). p-AKT expression was increased by 1.7-fold. The reduction of E-Cadherin expression, a known tumor-suppressor gene involved in cancer progression, was even more significant and became undetectable (Figure 3B). The expression of p53 was further reduced in the immortalized BVE–PTC cell line (about 40 passages) (Figure 4D). It has been reported that increased AKT signaling can negatively regulate p53 activity *via* AKT-mediated phosphorylation and activation of MDM2[29] and inhibit E-Cadherin expression.[30] The current data show that TSH can overcome $Braf^{V600E}$-induced senescence by downregulating p53 and E-Cadherin expression through upregulation of PI3K/AKT pathway, resulting in tumor progression.

Trp53 inactivation leads to ATC transformation and loss of $Braf^{V600E}$-induced senescence

To further confirm the role of p53 in $Braf^{V600E}$-induced senescence and tumor regression, we created two mouse strains: TPO–$Braf^{V600E}$–$Trp53^{-/-}$ (homozygous *Trp53* knockout) and TPO–$Braf^{V600E}$–$Trp53^{+/-}$ (heterozygous *Trp53* knockout) by crossing LSL–$Braf^{V600E}$ and TPO–Cre mice with TSG–p53. AtC development was observed from both *TPO–*$Braf^{V600E}$–$Trp53^{-/-}$ and TPO–$Braf^{V600E}$–$Trp53^{+/-}$, although there was a 2–3-month delay and tumors grow slower from TPO–$Braf^{V600E}$–$Trp53^{+/-}$ mice (the loss of WT p53 allele in the tumors was not observed). ATC transformation could be detected as early as 12 weeks (Figure 4A). Histologically, ATC were co-existed with PTC, and ATC tumors were larger from TPO–$Braf^{V600E}$–$Trp53^{-/-}$ mice than from TPO–$Braf^{V600E}$–$Trp53^{+/-}$ mice (Figure 4A). Characteristic features of ATC were present, such as undifferentiated cellular structure, pleomorphic giant cells and spindle cells. In contrast to BVE–PTC tumor transplants with wild-type *Trp53*, BVE–PTC tumor transplants with either homozygous or heterozygous *Trp53* knockout were able to continue to grow in nude mice without elevated serum TSH (Figure 4B). These data indicate that one allelic inactivation of *Trp53* is sufficient for ATC transformation and TSH-independent tumor growth. Histology of tumor transplants with *Trp53* knockout showed that PTC architecture was completely replaced by ATC architecture and lymphocyte infiltration was absent (Figure 4C, a and b) whereas, in primary tumors, both PTC and ATC components were present (Figure 4A). This may be due to the fact that only the ATC component from primary tumors could continue to grow in nude mice and the PTC component before transformation to ATC was unable to grow under normal serum TSH even though *Trp53* is inactivated, resulting in the enrichment of the ATC component.

The BVE–ATC cells from TPO–$Braf^{V600E}$–$Trp53^{-/-}$ tumor transplants could replicate in cell cultures without TSH and two cell lines were established: BVE–ATC-c1 and BVE–ATC-c2. As compared with the BVE–PTC cell line, p-AKT expression was significantly increased in both cell lines as a result of *Trp53* knockout (Figure 4D). The increased p-AKT expression in the normal thyroid cells is probably due to the presence of 2 mU/ml bovine

TSH in the primary thyroid cell culture. p-ERK levels were also elevated in ATC cells lines when compared with normal, but the level of increase was similar to that in BVE-PTC cell line (Figure 4D). These data indicate that PI3K/AKT pathway activation has an essential role in PTC-to-ATC transformation.

Effectiveness of simultaneous inhibition of both MAPK and PI3K/AKT pathways against ATC cells

Because both MAPK and PI3K/AKT pathways are activated in BVE–ATC cells, targeting both pathways may offer a better therapeutic outcome for ATC. To confirm the hypothesis, BVE–PTC and BVE–ATC-c1 cell lines were treated with PI3K inhibitor LY294002 or $BRAF^{V600E}$ inhibitor PLX4720 alone or in combination for short term (up to 72 h) and long term (14 days) effects on cell proliferation. The short-term effects on cell proliferation were determined by a non-radioactive MTS assay, and the long-term effects of PLX4720 and LY294002 inhibitors were measured by a colony formation assay. BVE–ATC cells became resistant to PLX4720 treatment (Figures 5A and B, $P < 0.01$). There were more than 60% of viable BVE–ATC cells after10 μM PLX4720 treatment for 72 h (Figure 5A) and 75% of viable cells after 4 μM PLX4720 treatment for 14 days (Figure 5B). By contrast, less than 30% and 50% of BVE–PTC cells were viable following 72 h treatment (10 μM) (Figure 5A) and 14-day treatment (4 μM) (Figure 5B), respectively. The resistance to PLX4720, however, could be reversed by combined treatment of PLX4720 and LY294002 inhibitors (Figures 5A and B). The viable BVE–ATC cells were reduced to 35% after combined PLX4720 and LY294002 treatment (10 μM each) for 72 h. The effects of combined treatment were even more obvious during long-term treatment using a lower concentration (4 μM) of each inhibitor: 35% from a combined treatment versus 74% from a single PLX4720 treatment (Figure 5B). These data demonstrate the synergistic effects of simultaneous targeting of both MAPK and PI3K/AKT pathways against ATC cells.

DISCUSSION

In the present study, we have demonstrated that OIS is initiated in the BVE–PTC tumors when serum TSH is normal and this process is dependent on normal p53 function. In addition, TSH can reduce p53 expression through upregulation of the PI3K/AKT pathway and inhibit OIS, resulting in tumor progression. Either homozygous or heterozygous inactivation of *Trp53* leads to the loss of OIS and promotes transformation of PTC into ATC with subsequently increased activation of the PI3K/AKT pathway. Furthermore, simultaneous targeting of both MAPK and PI3K/AKT pathways may offer a better therapeutic outcome against ATC. These data demonstrate the significant oncogenic role of TSH in thyroid tumor progression: with long-term TSH stimulation, thyroid cancer cells can overcome OIS, gradually become TSH-independent and progress into poorly differentiated cancer.

OIS is a tumor-suppressive mechanism against oncogenic events.[31] Two major pathways are involved in the process: $p16^{INK4A}$–Rb and ARF–p53.[32] Unlike replicative senescence, OIS cannot be bypassed by the expression of hTERT,[33] but can be bypassed by inactivation of the $p16^{INK4A}$–Rb or ARF–p53 pathway.[32] Previous studies have demonstrated that

mutations in oncogenes (*Ras* and *Braf* and tumor-suppressor genes (*Pten* and *NF1*) can trigger OIS *in vivo* in human tumors and in mouse tumor models,[31,34–36] and is dose-dependent.[37] For example, low levels of *Ras* activation stimulate cellular proliferation and mammary epithelial hyperplasias, whereas high levels of *Ras* activation induce cellular senescence.[37] Heterozygous *Pten* inactivation promotes tumor initiation and proliferation,[38] whereas homozygous loss of *Pten* inhibits prostate tumorigenesis by triggering a powerful p53-dependent cellular senescence.[35] Although senescence occurs mainly in benign tumors to prevent the progression of benign lesions into malignant tumors,[18,36,39] evidence of cellular senescence in early-stage human prostate cancer has also been shown and is p53-dependent.[35] Vizioli *etal*.[40] have reported evidence of OIS in human primary thyrocytes and thyroid cancers. In thyroid cancer, the expression of OIS markers such as $p16^{INK4A}$, $p21^{CIP1/WAF1}$ and IGFBP7 is upregulated at early stages and lost during thyroid tumor progression. Although p53 expression is not investigated in thyroid cancer specimens, its expression is induced following $Braf^{V600E}$ transfection in primary thyrocytes.[40] The current study has shown that OIS can even occur *in vivo* in advanced PTC and can be triggered by decreased serum TSH and activation of p53. To our knowledge, this is the first report demonstrating the induction of OIS in advanced tumors. Conventional chemotherapy and radiotherapy also induce cellular senescence in tumors but with significant side effects of cytotoxicity to normal tissues. Treatments aimed at the induction of OIS such as controlling serum TSH, blocking the TSH signaling pathway or stabilizing p53 function may be the cost-effective approach in thyroid cancer therapy, at least for well-differentiated thyroid cancers without p53 mutation. However, these interventions become ineffective when normal p53 function is disrupted, for example, by somatic mutations. Indeed, heterozygous p53 mutation is frequently found in ATC patients who are often non-responsive to TSH-suppressive therapy,[41] and less commonly in well-differentiated thyroid cancers.[42]

$Braf^{V600E}$-induced senescence in benign human naevi occurs through the activation of the $p16^{INK4A}$–Rb pathway,[18] whereas, in benign lung tumors, the ARF–p53 pathway is activated.[43] Recently, it has been shown that $p16^{INK4A}$–Rb pathway is involved in the *RAS*-induced senescence in human thyrocytes.[44] Utilization of the cellular senescence pathway is likely cell-type-specific and probably oncogene-specific. It has been reported that *NF1, Pten, Raf* or *Ras* mutations can induce a negative feedback response and promote senescence by inhibiting the PI3K/AKT pathway activated by these mutations.[36,45] In mouse prostate cancer, the growth arrest induced by complete *Pten* inactivation is through the p53-dependent pathway.[35] Although *Trp53* inactivation fails to produce a tumor phenotype, complete *Pten* inactivation triggers OIS, resulting in non-lethal invasive prostate cancer after long latency. When both *Pten* and *Trp53* are inactivated, OIS is lost and lethal invasive prostate cancer develops at a young age.[35] In mouse thyroid, *Pten* inactivation causes only benign goiter and follicular adenoma,[46] whereas combined inactivation of *Trp53* and *Pten* results in follicular thyroid cancer and ATC, the most lethal forms of thyroid cancer.[47] Although OIS is not explored in those studies, the p53-dependent cellular senescence pathway is likely involved in preventing the progression of benign goiter and follicular adenoma into follicular thyroid cancer and ATC. McFadden *et al*.[48] have reported recently that homozygous deletion of *Trp53* leads to accelerated progression of PTC to ATC and TSH suppression does not affect tumor progression to ATC in a similar model. Their data

are in agreement with our finding that tumor growth will become TSH-independent and likely to progress to ATC when p53 is inactivated. The current study further demonstrates that heterozygous deletion of *Trp53* in the context of $Braf^{V600E}$could also result in ATC transformation, and is sufficient to reverse OIS, indicating haplotype insufficiency of *Trp53* to counter ATC transformation. This is consistent with clinical studies that heterozygous, not homozygous, *TP53* mutations are often found in ATC patients and cell lines.[41,49] The large lymphocyte infiltration and increased secretion of inflammatory cytokines and chemokines from the senescent tumor cells suggests that OIS can trigger an innate immune response to enhance tumor regression and clearance, and this process is dependent on functional *Trp53*. Indeed, upregulation of inflammatory cytokines and an innate immune response has been shown in p53-induced cellular senescence in mouse liver cancer.[50]

Activation of the PI3K/AKT pathway not only has a key role in tumor progression, but it also triggers OIS to maintain the balance of growth. In ATC, $BRAF^{V600E}$ is frequently found together with either gain-of-function mutations in the p110 catalytic subunit of PI3K (*PIK3CA*) or loss-of-function mutations in *TP53*. Charles *et al*.[51] have shown that mice carrying an activated $PIK3CA^{H1047R}$ are unable to develop tumor. However, concomitant mutations of both $PIK3CA^{H1047R}$ and $BRAF^{V600E}$ lead to ATC, suggesting that single activation mutation in either MAPK or PI3K pathway may trigger OIS, whereas concomitant mutations in both pathways would likely neutralize OIS, leading to ATC development. We have identified in the current study that elevated serum TSH or *Trp53* mutation could override OIS, resulting in tumor progression. PTEN is a key negative regulator of PI3K/AKT signaling and can increase p53 expression.[52,53] Induction of cellular senescence as a novel therapeutic approach against prostate cancer has been demonstrated.[45] In the presence of functional p53, the PTEN inhibitor VO-OHpic[54] induces senescence, whereas the Mdm2 inhibitor Nutlin-3, a p53-stabilizing drug,[55] enhances senescence by super-activation of p53.[45] These may represent a viable approach for thyroid cancer patients who are not responsive to TSH-suppressive therapy, but have functional p53 or PTEN. In the absence of functional p53, simultaneous targeting of both MAPK and PI3K/AKT pathways may offer a better therapeutic outcome.

MATERIALS AND METHODS

Mice

LSL–$Braf^{V600E}$, TPO–Cre and TSG–p53 strains have been described previously.[56–58] LSL–$Braf^{V600E}$ mice carry a latent mutant allele of *Braf* and are kept as heterozygotes. LSL–$Braf^{V600E}$ was crossed with TPO–Cre mice to generate the TPO–$Braf^{V600E}$ strain where $Braf^{V600E}$ is exclusively expressed in thyroid follicular cells under its native promoter through Cre-recombinase-mediated deletion of a floxed transcriptional stop sequence. The resulting TPO–$Braf^{V600E}$ strain expressed mutant $Braf^{V600E}$ transcripts at a physiological level. TSG–p53 (*Trp53* knockout, B6.129–$Trp53^{tm1Brd}$ N12) mice were obtained from Taconic (Hudson, NY, USA). To knockout *Trp53* in TPO–$Braf^{V600E}$ mice, TSG–p53 mice were first crossed with LSL–$Braf^{V600E}$ or TPO–Cre mice to generate $Trp53^{+/-}$; $Braf^{V600E}$ strain or TPO–Cre; $Trp53^{+/-}$ strain. $Trp53^{+/-}$; $Braf^{V600E}$ mice and TPO–Cre; $Trp53^{+/-}$ mice were then bred together to create TPO–$Braf^{V600E}$–$Trp53^{-/-}$ (homozygous *Trp53* knockout)

or TPO–*Braf*^{V600E}–*Trp53*$^{+/-}$ (heterozygous *Trp53* knockout) mice. Female athymic BALB/c-nu/nu mice (4–8 weeks of age) were acquired from the Jackson Laboratory (Bar Harbor, ME, USA). Mice were provided with autoclaved food and water *ad libitum*. The number of animals was determined by the formula: $n = \log \beta / \log p$; where β is the probability of committing a Type II error (0.05) and p represents the proportion of the animals in the group that have no tumor regression. If tumor regression expected to occur in 30% with 95% chance of detecting the regression, the number of animals needed: $n = \log 0.05 / \log 0.7 = 8.4$. Thus, nine animals need to be used. We used 16 animals in the study. The animals were randomly chosen and divided into control and experimental groups. No blinding was carried out. The study was approved by the Animal Care and Usage Committee of the institution and conducted in compliance with the Public Health Service Guidelines for the Care and Use of Animals in Research.

Genotyping of transgenic mice

Genotyping of Cre-mediated recombination of the LSL–*Braf*^{V600E} targeted allele has been described previously.[57] Briefly, the following primers were used to detect LSL–*Braf*^{V600E} recombination in the mouse tissue: primer A, 5′-AGTCAATCATCCACAGAGACCT-3′, primer B: 5′-GCTTGGCTGGACGTAAACTC-3′, and primer C, 5′-GCCCAGGCTCTTTATGAGAA-3′. Primers A+C detect the wild-type allele (466 bp) and Cre-recombined allele (Lox-*Braf*^{V600E}) yielding a 518-bp fragment. Primers B+C detect the LSL–*Braf*^{V600E} allele (140 bp). For genotyping of wild-type and mutant *Trp53*, the following primers were used: p53-X5, 5′-TAAGTCAGAAGCCGGGAGATGG-3′, p53-X3, 5′-AGCCTGAGCATGGAAGTAAGAC-3′, and NEO-19, 5′-CTATCAGGACATAGCGTTGG-3′. p53-X5 and p53-X3 detect wild-type *Trp53* yielding a 680-bp fragment. p53-X5 and NEO-19 detect mutant *Trp53* yielding a 320-bp fragment. PCR conditions are 95 °C for 5 min followed by 35 cycles of amplification (95 °C for 1 min, 60 °C for 1 min, 72 °C for 1 min with a final extension at 72 °C for 10 min).

Normal thyroid and tumor cell culture

Normal thyroids and thyroid tumors were collected aseptically from donor mice (TPO–*Braf*^{WT}, TPO–*Braf*^{7600E} and TPO–*Braf*^{V600E}–*Trp53*$^{-/-}$) using blunt dissection, mechanically dissociated by mincing and passing through a 40-μM mesh sterile screen, and suspended in DMEM/F12 growth medium (10% fetal bovine serum, 100 units/ml penicillin, 100 μg/ml streptomycin). Cells were further dissociated by incubation in the growth medium containing 100 U/ml type I collagenase (Sigma-Aldrich, St Louis, MO, USA) and 1.0 U/ml dispase I (Roche Diagnostics, Indianapolis, IN, USA) at 37 °C in a rocking water bath for 60 min. The cell suspension was washed twice and re-suspended in a 10-mm culture dish with DMEM/F12 growth medium containing 2 mU/ml bovine TSH (Sigma-Aldrich) to establish a primary normal thyroid culture or a BVE–PTC cell line. Two BVE–ATC cell lines (BVE–ATC-c1 and BVE–ATC-c2) were established from TPO–*Braf*^{V600E}μ*Trp53*$^{-/-}$ tumor transplants by limited dilution and subcloning, and cultured in DMEM/F12 growth medium without bovine TSH. Their genetic background was confirmed by genotyping.

Tumor transplants

To evaluate tumor progression under normal and high serum TSH, thyroid tumors were removed aseptically from TPO–$Braf^{V600E}$ mice at 4–6 months of age and were implanted subcutaneously on the flank of nude mice ($n = 8$), TPO–$Braf^{V600E}$ ($n = 8$) or their wild-type littermates ($n = 8$, TPO–$Braf^{WT}$) under general anesthesia using a ketamine/xylazine combination (80 mg/kg:10 mg/kg, intraperitoneally). The incision was closed with sutures and tumor growth was monitored weekly. All animals were maintained in a sterile environment on a daily 12-h light/12-h dark cycle. To evaluate tumor progression with *Trp53* knockout, thyroid tumors were removed from TPO–$Braf^{V600E}$–$Trp53^{-/-}$ mice or TPO–$Braf^{V600E}$–$Trp53^{+/-}$ at 3 months of age and were implanted subcutaneously on the flank of eight nude mice in each group under the same procedure as above. The genetic background of tumor transplants was confirmed by genotyping.

TSH and cytokine/chemokine measurements

Blood was collected by cardiac puncture. Serum TSH was measured by Luminex's xMAP using a MILLIPLEX MAP Mouse Pituitary Magnetic Bead Panel following the manufacturer's instructions (MPTMAG-49K, EMD Millipore Corporation, Billerica, MA, USA). Cytokines and chemokines in the culture medium and tumor fluid were measured by Luminex's xMAP using a MILLIPLEX MAP Mouse Cytokine/Chemokine Magnetic Bead Panel—Premixed 32 Plex (MCYTMAG-70K-PX32). The following 32 cytokine and chemokine levels were determined: VEGF, Eotaxin, G-CSF, GM-CSF, IFN-γ, IL-1α, IL-1β, IL-2, IL-3, IL-4, IL-5, IL-6, IL-7, IL-9, IL-10, IL-12 (p40), IL-12 (p70), IL-13, IL-15, IL-17, IP-10, KC-like, LIF, LIX, MCP-1, M-CSF, MIG, MIP-1α, MIP-1β, MIP-2, RANTES and TNF-α.

Histology and immunohistochemistry

Histology and immunohistochemical staining were described previously.[59] Briefly, 4-μm-thick formalin-fixed paraffin-embedded tissue sections were prepared and stained with hematoxylin and eosin, Ki-67 (1:400 dilution) or p53 (1:100 dilution) using a DAKO LSAB +kit (DAKO, Carpinteria, CA, USA). Ki-67 and p53 antibodies were obtained from Cell Signaling Technology, Danvers, MA, USA.

Senescence-associated expression of beta-galactosidase (SA-beta-Gal) activity

SA-beta-Gal activity was detected using an Abcam's Senescence Detection Kit following the manufacturer's procedure (Abcam, Cambridge, MA, USA).

Western blot analysis

Cell lysates were obtained by extraction in RIPA buffer (20 mM Tris-HCl, pH7.4, 150 mM NaCl, 5 mM EDTA, 1% NP-40) containing Pierce's Halt Protease Inhibitor Cocktail (Thermo Scientific, Rockford, IL, USA). Protein concentration was determined by Bradford's assay using a Bio-Rad protein assay kit (Bio-Rad, Hercules, CA, USA). Proteins (40 μg) were loaded onto a 12% sodium dodecyl sulfate–polyacrylamide gel. Proteins were transferred to a polyvinyl difluoride membrane and subjected to western blot analysis using the following antibodies from either Cell Signaling Technology (Boston, MA, USA): p53

(cat# 2524), phospho-ERK1/2 (cat# 4370), E-Cadherin (cat# 3195), phospho-AKT (cat# 4060), total-ERK1/2 (cat# 9102), total-AKT (cat# 9272) and β-actin (cat# 4970) or Santa Cruz Biotechnology (Dallas, TX, USA): $p16^{INK4A}$ (cat# sc-1207) and $p21^{CIP1/WAF1}$ (cat# sc-397). All antibodies were used at 1:1000 dilutions except for total-ERK1/2, total-AKT and β-actin where 1:5000 dilutions were used. Quantification of western blots was performed using ImageJ software (http://rsb.info.nih.gov/ij/).

Cell proliferation assay

Cell proliferation was measured by a non-radioactive MTS assay kit according to the manufacturer's procedure (Promega Corp, Madison, WI, USA). Briefly, cells were plated in triplicate into 96-well plates (1×10^3 cells/well) containing 10% serum and different concentrations of PLX4720 (selective $BrafV^{600E}$ inhibitor), LY294002 (PI3K inhibitor) or both for up to 72 h (Selleck Chemicals, Houston, TX, USA). For the final 4 h of incubation, 20 μl of CellTiter 96 AQ_{ueous} One Solution reagent were added into each well for measurement of cell viability.

Colony formation assay

Cells were plated into 12-well plates ($\times 10^2$ cells/well) and cultured for 14 days in the absence or presence of different concentrations of PLX4720, LY294002 or both. Cells were then fixed with methanol for 10 min and stained with 0.5% crystal violet dye (in methanol:de-ionized water, 1:5) for 10 min. After three washes with de-ionized water to remove excess crystal violet dye, the crystal violet dye was released from cells by incubation with 1% sodium dodecyl sulfate for 2 h before optical density $(OD)_{570\ nm}$ measurement.

Statistical analysis

Unpaired Student's *t*-test (two-tailed) was used. A *P* value of 0.05 or less was considered significant.

ACKNOWLEDGEMENTS

We would like to thank Mr Wilfredo Antiquera for excellent technical support. This study is supported by KACST grant 11-BIO1434-20.

REFERENCES

1. Davies L, Welch HG. Increasing incidence of thyroid cancer in the United States, 1973-2002. JAMA 2006; 295: 2164–2167. [PubMed: 16684987]
2. Hundahl SA, Fleming ID, Fremgen AM, Menck HR. A National Cancer Data Base report on 53,856 cases of thyroid carcinoma treated in the U.S., 1985-1995 [see commetns]. Cancer 1998; 83: 2638–2648. [PubMed: 9874472]
3. Cooper DS, Doherty GM, Haugen BR, Kloos RT, Lee SL, Mandel SJ et al. Revised American Thyroid Association management guidelines for patients with thyroid nodules and differentiated thyroid cancer. Thyroid 2009; 19: 1167–1214. [PubMed: 19860577]
4. Mazzaferri EL, Kloos RT. Clinical review 128: Current approaches to primary therapy for papillary and follicular thyroid cancer. J Clin Endocrinol Metab 2001; 86: 1447–1463. [PubMed: 11297567]
5. Hollenbeak CS, Boltz MM, Schaefer EW, Saunders BD, Goldenberg D. Recurrence of differentiated thyroid cancer in the elderly. Eur J Endocrinol 2013; 168: 549–556. [PubMed: 23337385]

6. Durante C, Haddy N, Baudin E, Leboulleux S, Hartl D, Travagli JP et al. Long-term outcome of 444 patients with distant metastases from papillary and follicular thyroid carcinoma: benefits and limits of radioiodine therapy. J Clin Endocrinol Metab 2006; 91: 2892–2899. [PubMed: 16684830]
7. Xing M BRAF mutation in thyroid cancer. Endocr Relat Cancer 2005; 12: 245–262. [PubMed: 15947100]
8. Romei C, Ciampi R, Faviana P, Agate L, Molinaro E, Bottici V et al. BRAFV600E mutation, but not RET/PTC rearrangements, is correlated with a lower expression of both thyroperoxidase and sodium iodide symporter genes in papillary thyroid cancer. Endocr Relat Cancer 2008; 15: 511–520. [PubMed: 18509003]
9. Durante C, Puxeddu E, Ferretti E, Morisi R, Moretti S, Bruno R et al. BRAF mutations in papillary thyroid carcinomas inhibit genes involved in iodine metabolism. J Clin Endocrinol Metab 2007; 92: 2840–2843. [PubMed: 17488796]
10. Haymart MR, Glinberg SL, Liu J, Sippel RS, Jaume JC, Chen H. Higher serum TSH in thyroid cancer patients occurs independent of age and correlates with extrathyroidal extension. Clin Endocrinol (Oxf) 2009; 71: 434–439. [PubMed: 19067720]
11. Boelaert K, Horacek J, Holder RL, Watkinson JC, Sheppard MC, Franklyn JA. Serum thyrotropin concentration as a novel predictor of malignancy in thyroid nodules investigated by fine-needle aspiration. J Clin Endocrinol Metab 2006; 91: 4295–4301. [PubMed: 16868053]
12. Fiore E, Rago T, Provenzale MA, Scutari M, Ugolini C, Basolo F et al. Lower levels of TSH are associated with a lower risk of papillary thyroid cancer in patients with thyroid nodular disease: thyroid autonomy may play a protective role. Endocr Relat Cancer 2009; 16: 1251–1260. [PubMed: 19528244]
13. Jonklaas J, Nsouli-Maktabi H, Soldin SJ. Endogenous thyrotropin and triiodothyronine concentrations in individuals with thyroid cancer. Thyroid 2008; 18:943–952. [PubMed: 18788918]
14. Knauf JA, Ma X, Smith EP, Zhang L, Mitsutake N, Liao XH et al. Targeted expression of BRAFV600E in thyroid cells of transgenic mice results in papillary thyroid cancers that undergo dedifferentiation. Cancer Res 2005; 65: 4238–4245. [PubMed: 15899815]
15. Franco AT, Malaguarnera R, Refetoff S, Liao XH, Lundsmith E, Kimura S et al. Thyrotrophin receptor signaling dependence of Braf-induced thyroid tumor initiation in mice. Proc Natl Acad Sci USA 2011; 108: 1615–1620. [PubMed: 21220306]
16. Charles RP, Iezza G, Amendola E, Dankort D, McMahon M. Mutationally activated BRAF(V600E) elicits papillary thyroid cancer in the adult mouse. Cancer Res 2011; 71: 3863–3871. [PubMed: 21512141]
17. Shimamura M, Nakahara M, Orim F, Kurashige T, Mitsutake N, Nakashima M et al. Postnatal expression of BRAFV600E does not induce thyroid cancer in mouse models of thyroid papillary carcinoma. Endocrinology 2013; 154: 4423–4430. [PubMed: 23970782]
18. Michaloglou C, Vredeveld LC, Soengas MS, Denoyelle C, Kuilman T, van der Horst CM et al. BRAFE600-associated senescence-like cell cycle arrest of human naevi. Nature 2005; 436: 720–724. [PubMed: 16079850]
19. Dhomen N, Reis-Filho JS, da Rocha Dias S, Hayward R, Savage K, Delmas V et al. Oncogenic Braf induces melanocyte senescence and melanoma in mice. Cancer Cell 2009; 15: 294–303. [PubMed: 19345328]
20. Fiore E, Vitti P. Serum TSH and risk of papillary thyroid cancer in nodular thyroid disease. J Clin Endocrinol Metab 2012; 97: 1134–1145. [PubMed: 22278420]
21. Boelaert K The association between serum TSH concentration and thyroid cancer. Endocr Relat Cancer 2009; 16: 1065–1072. [PubMed: 19620248]
22. Fiore E, Rago T, Provenzale MA, Scutari M, Ugolini C, Basolo F et al. L-thyroxine-treated patients with nodular goiter have lower serum TSH and lower frequency of papillary thyroid cancer: results of a cross-sectional study on 27 914 patients. Endocr Relat Cancer 2010; 17: 231–239. [PubMed: 20167722]
23. Natori T, Sata M, Washida M, Hirata Y, Nagai R, Makuuchi M. G-CSF stimulates angiogenesis and promotes tumor growth: potential contribution of bone marrow-derived endothelial progenitor cells. Biochem Biophys Res Commun 2002; 297: 1058–1061. [PubMed: 12359263]

24. Li X, Yang Q, Yu H, Wu L, Zhao Y, Zhang C et al. LIF promotes tumorigenesis and metastasis of breast cancer through the AKT-mTOR pathway. Oncotarget 2014; 5: 788–801. [PubMed: 24553191]
25. Fujisawa T, Joshi BH, Puri RK. IL-13 regulates cancer invasion and metastasis through IL-13Ralpha2 via ERK/AP-1 pathway in mouse model of human ovarian cancer. Int J Cancer 2012; 131: 344–356. [PubMed: 21858811]
26. Hagemann T, Robinson SC, Thompson RG, Charles K, Kulbe H, Balkwill FR. Ovarian cancer cell-derived migration inhibitory factor enhances tumor growth, progression, and angiogenesis. Mol Cancer Ther 2007; 6: 1993–2002. [PubMed: 17620429]
27. Kollmar O, Junker B, Rupertus K, Scheuer C, Menger MD, Schilling MK. Liver resection-associated macrophage inflammatory protein-2 stimulates engraftment but not growth of colorectal metastasis at extrahepatic sites. J Surg Res 2008; 145: 295–302. [PubMed: 17561115]
28. Yoshimura T, Howard OM, Ito T, Kuwabara M, Matsukawa A, Chen K et al. Monocyte chemoattractant protein-1/CCL2 produced by stromal cells promotes lung metastasis of 4T1 murine breast cancer cells. PLoS One 2013; 8: e58791. [PubMed: 23527025]
29. Zhou BP, Liao Y, Xia W, Zou Y, Spohn B, Hung MC. HER-2/neu induces p53 ubiquitination via Akt-mediated MDM2 phosphorylation. Nat Cell Biol 2001; 3:973–982. [PubMed: 11715018]
30. Cheng JC, Auersperg N, Leung PC. Inhibition of p53 induces invasion of serous borderline ovarian tumor cells by accentuating PI3K/Akt-mediated suppression of E-cadherin. Oncogene 2011; 30: 1020–1031. [PubMed: 20972462]
31. Courtois-Cox S, Jones SL, Cichowski K. Many roads lead to oncogene-induced senescence. Oncogene 2008; 27: 2801–2809. [PubMed: 18193093]
32. Serrano M, Lin AW, McCurrach ME, Beach D, Lowe SW. Oncogenic ras provokes premature cell senescence associated with accumulation of p53 and p16INK4a. Cell 1997; 88: 593–602. [PubMed: 9054499]
33. Wei S, Sedivy JM. Expression of catalytically active telomerase does not prevent premature senescence caused by overexpression of oncogenic Ha-Ras in normal human fibroblasts. Cancer Res 1999; 59: 1539–1543. [PubMed: 10197626]
34. Braig M, Lee S, Loddenkemper C, Rudolph C, Peters AH, Schlegelberger B et al. Oncogene-induced senescence as an initial barrier in lymphoma development. Nature 2005; 436: 660–665. [PubMed: 16079837]
35. Chen Z, Trotman LC, Shaffer D, Lin HK, Dotan ZA, Niki M et al. Crucial role of p53-dependent cellular senescence in suppression of Pten-deficient tumorigenesis. Nature 2005; 436: 725–730. [PubMed: 16079851]
36. Courtois-Cox S, Genther Williams SM, Reczek EE, Johnson BW, McGillicuddy LT, Johannessen CM et al. A negative feedback signaling network underlies oncogene-induced senescence. Cancer Cell 2006; 10: 459–472. [PubMed: 17157787]
37. Sarkisian CJ, Keister BA, Stairs DB, Boxer RB, Moody SE, Chodosh LA. Dose-dependent oncogene-induced senescence in vivo and its evasion during mammary tumorigenesis. Nat Cell Biol 2007; 9: 493–505. [PubMed: 17450133]
38. Di Cristofano A, Pesce B, Cordon-Cardo C, Pandolfi PP. Pten is essential for embryonic development and tumour suppression. Nat Genet 1998; 19: 348–355. [PubMed: 9697695]
39. Collado M, Gil J, Efeyan A, Guerra C, Schuhmacher AJ, Barradas M et al. Tumour biology: senescence in premalignant tumours. Nature 2005; 436: 642. [PubMed: 16079833]
40. Vizioli MG, Possik PA, Tarantino E, Meissl K, Borrello MG, Miranda C et al. Evidence of oncogene-induced senescence in thyroid carcinogenesis. Endocr Relat Cancer 2011; 18: 743–757. [PubMed: 21937739]
41. Fagin JA, Matsuo K, Karmakar A, Chen DL, Tang SH, Koeffler HP. High prevalence of mutations of the p53 gene in poorly differentiated human thyroid carcinomas. J Clin Invest 1993; 91: 179–184. [PubMed: 8423216]
42. Malaguarnera R, Vella V, Vigneri R, Frasca F. p53 family proteins in thyroid cancer. Endocr Relat Cancer 2007; 14: 43–60. [PubMed: 17395974]

43. Dankort D, Filenova E, Collado M, Serrano M, Jones K, McMahon M. A new mouse model to explore the initiation, progression, and therapy of BRAFV600E-induced lung tumors. Genes Dev 2007; 21: 379–384. [PubMed: 17299132]
44. Vizioli MG, Santos J, Pilotti S, Mazzoni M, Anania MC, Miranda C et al. Oncogenic RAS-induced senescence in human primary thyrocytes: molecular effectors and inflammatory secretome involved. Oncotarget 2014; 5: 8270–8283. [PubMed: 25268744]
45. Alimonti A, Nardella C, Chen Z, Clohessy JG, Carracedo A, Trotman LC et al. A novel type of cellular senescence that can be enhanced in mouse models and human tumor xenografts to suppress prostate tumorigenesis. J Clin Invest 2010; 120: 681–693. [PubMed: 20197621]
46. Yeager N, Klein-Szanto A, Kimura S, Di Cristofano A. Pten loss in the mouse thyroid causes goiter and follicular adenomas: insights into thyroid function and Cowden disease pathogenesis. Cancer Res 2007; 67: 959–966. [PubMed: 17283127]
47. Antico Arciuch VG, Russo MA, Dima M, Kang KS, Dasrath F, Liao XH et al. Thyrocyte-specific inactivation of p53 and Pten results in anaplastic thyroid carcinomas faithfully recapitulating human tumors. Oncotarget 2011; 2: 1109–1126. [PubMed: 22190384]
48. McFadden DG, Vernon A, Santiago PM, Martinez-McFaline R, Bhutkar A, Crowley DM et al. p53 constrains progression to anaplastic thyroid carcinoma in a Brafmutant mouse model of papillary thyroid cancer. Proc Natl Acad Sci USA 2014; 111: E1600–E1609. [PubMed: 24711431]
49. Zou M, Baitei EY, Alzahrani AS, BinHumaid FS, Alkhafaji D, Al-Rijjal RA et al. Concomitant RAS, RET/PTC, or BRAF mutations in advanced stage of papillary thyroid carcinoma. Thyroid 2014; 24: 1256–1266. [PubMed: 24798740]
50. Xue W, Zender L, Miething C, Dickins RA, Hernando E, Krizhanovsky V et al. Senescence and tumour clearance is triggered by p53 restoration in murine liver carcinomas. Nature 2007; 445: 656–660. [PubMed: 17251933]
51. Charles RP, Silva J, Iezza G, Phillips WA, McMahon M. Activating BRAF and PIK3CA mutations cooperate to promote anaplastic thyroid carcinogenesis. Mol Cancer Res 2014; 12: 979–986. [PubMed: 24770869]
52. Freeman DJ, Li AG, Wei G, Li HH, Kertesz N, Lesche R et al. PTEN tumor suppressor regulates p53 protein levels and activity through phosphatase-dependent and-independent mechanisms. Cancer Cell 2003; 3: 117–130. [PubMed: 12620407]
53. Mayo LD, Dixon JE, Durden DL, Tonks NK, Donner DB. PTEN protects p53 from Mdm2 and sensitizes cancer cells to chemotherapy. J Biol Chem 2002; 277: 5484–5489. [PubMed: 11729185]
54. Rosivatz E, Matthews JG, McDonald NQ, Mulet X, Ho KK, Lossi N et al. A small molecule inhibitor for phosphatase and tensin homologue deleted on chromosome 10 (PTEN)ACS Chem Biol 2006; 1: 780–790. [PubMed: 17240976]
55. Vassilev LT, Vu BT, Graves B, Carvajal D, Podlaski F, Filipovic Z et al. In vivo activation of the p53 pathway by small-molecule antagonists of MDM2. Science 2004; 303: 844–848. [PubMed: 14704432]
56. Kusakabe T, Kawaguchi A, Kawaguchi R, Feigenbaum L, Kimura S. Thyrocyte-specific expression of Cre recombinase in transgenic mice. Genesis 2004; 39: 212–216. [PubMed: 15282748]
57. Mercer K, Giblett S, Green S, Lloyd D, DaRocha Dias S, Plumb M et al. Expression of endogenous oncogenic V600EB-raf induces proliferation and developmental defects in mice and transformation of primary fibroblasts. Cancer Res 2005; 65: 11493–11500. [PubMed: 16357158]
58. Donehower LA, Harvey M, Slagle BL, McArthur MJ, Montgomery CA, Jr, Butel JS et al. Mice deficient for p53 are developmentally normal but susceptible to spontaneous tumours. Nature 1992; 356: 215–221. [PubMed: 1552940]
59. Zou M, Al-Baradie RS, Al-Hindi H, Farid NR, Shi Y. S100A4 (Mts1) gene overexpression is associated with invasion and metastasis of papillary thyroid carcinoma. Br J Cancer 2005; 93: 1277–1284. [PubMed: 16265347]

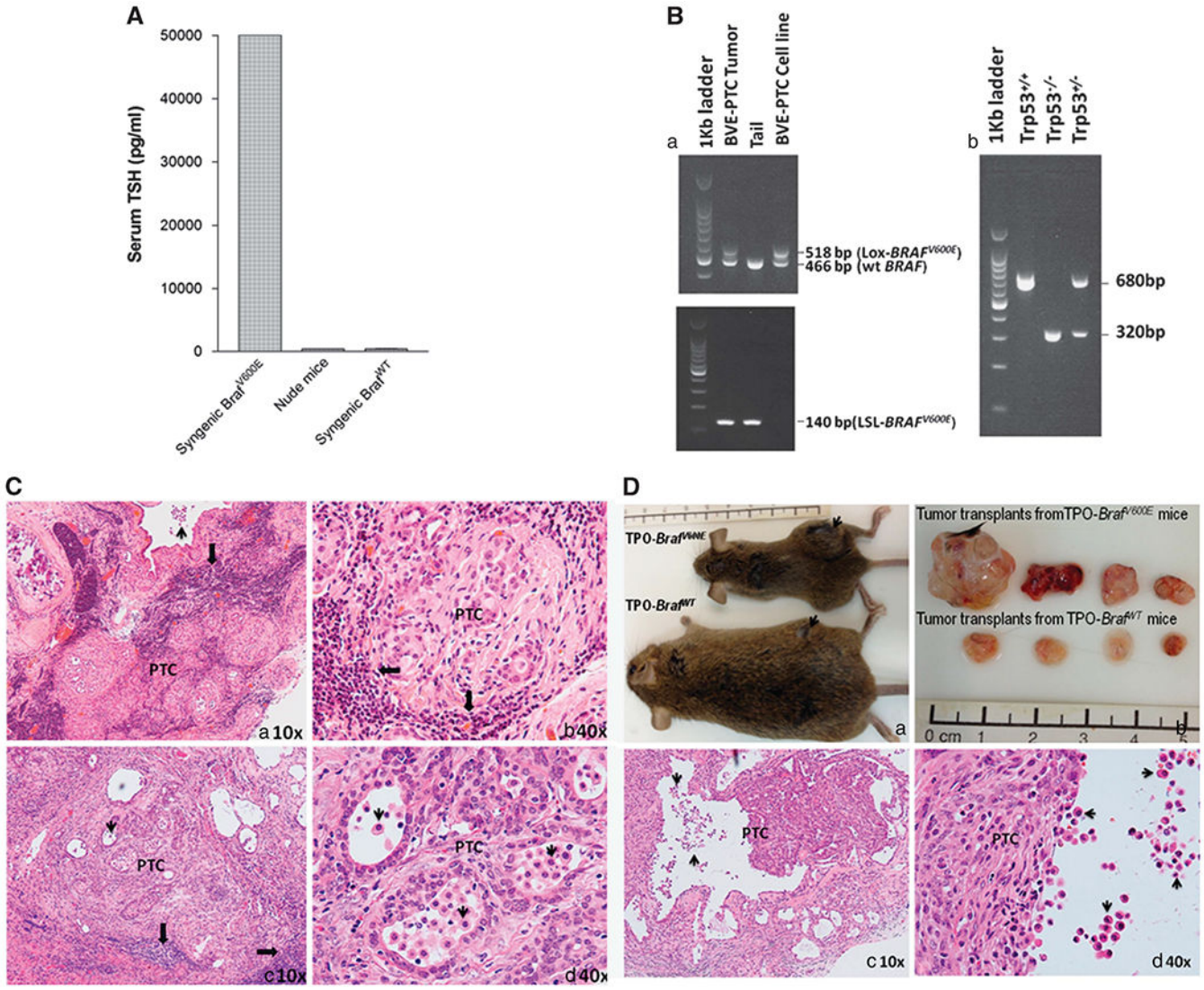

Figure 1.

Regression of BVE–PTC transplants in nude and TPO–*Braf*^{WT} mice. (**A**) Serum TSH level from TPO–*Braf*^{V600E}, TPO–*Braf*^{WT} and nude mice. The serum TSH levels from five TPO–*Braf*^{V600E} mice (5 months old) are all above the detection limit of 50 000 pg/ml. The average TSH levels from five TPO–*Braf*^{WT} and five nude mice of same age are 439.6 ± 39.8 and 426.4 ± 9.6 pg/ml, respectively. (**B**) Genotyping of TPO–*Braf*^{V600E} (a) and TPO–*Braf*^{V600E}–*Trp53*$^{-/-}$ mice (b). The PCR product was run on a 1.5% agarose gel. The LSL–*Braf*^{V600E} was recombined only in the thyroid (activation of *Braf*^{V600E}) as a result of Cre-mediated deletion of a floxed transcriptional stop sequence. The LSL-*Braf*^{V600E} allele was not detected in the BVE-PTC cell line, indicating complete Cre-mediated recombination in the thyroid tumor cell line (a, lower panel), and no fibroblast contamination. Wild-type and mutant *Trp53* alleles from BVE–PTC tumors are shown by 680-bp and 320-bp fragments, respectively. (**C**) Histology of BVE–PTC transplants. Tumors from 4- to 6-month-old TPO–*Braf*^{V600E} mice were transplanted subcutaneously into nude and TPO–*Braf*^{WT} mice. They were removed for histology after 4–7 months. The tumor transplants are surrounded by

heavy lymphocyte infiltration (indicated by dark arrows) from both nude mice (a and b) and TPO–$Braf^{WT}$ mice (c and d). Macrophages are often present in the empty spaces of tumor tissue (indicated by light arrows). (**D**) Tumor growth in TPO–$Braf^{V600E}$ mice. TPO–$Braf^{V600E}$ mice are about the half size of TPO–$Braf^{WT}$ mice due to severe hypothyroidism and tumor transplants are indicated by arrows (a). The size of tumor transplants after 4-month implantation in TPO–$Braf^{V600E}$ and TPO–$Braf^{WT}$ mice (b). Histology of tumor transplants from TPO–$Braf^{V600E}$ mice (c and d). There is more tumor tissue and less lymphocyte infiltration. Macrophages in the empty spaces of tumor tissue are indicated by light arrows.

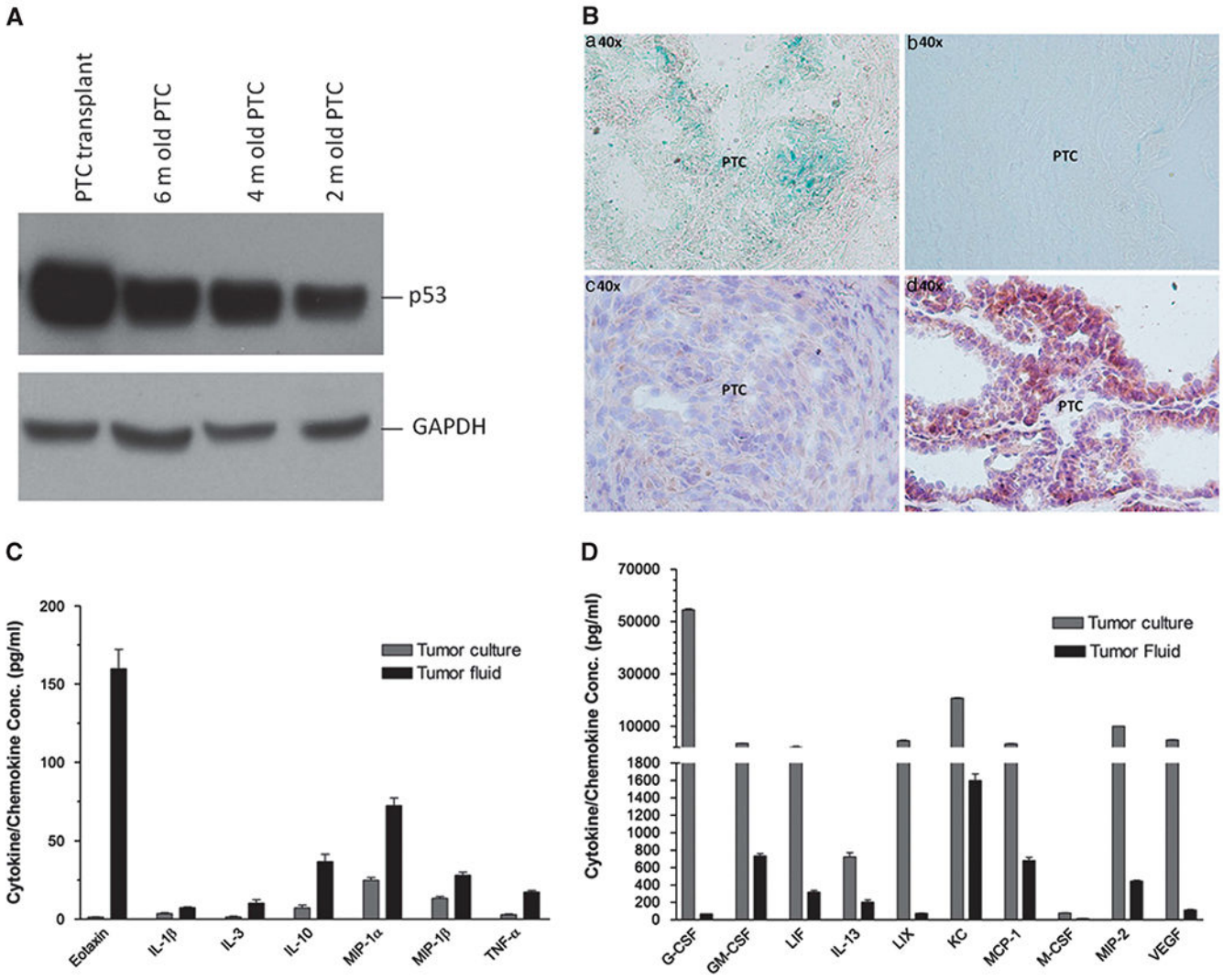

Figure 2.

Braf^{V600E}-induced senescence in BVE–PTC transplants. (**A**) Western blot analysis of p53 expression from a 6-month-old BVE–PTC tumor transplant and primary BVE–PTC tumors of different ages. The expression of p53 is significantly higher in the tumor transplants. There is also a gradual increase in p53 expression from primary BVE–PTC tumors: lower expression in early tumors and higher expression in late tumors. Quantification of the western blot was performed using ImageJ software. (**B**) Strong SA-beta-Gal staining (blue color, a) and no Ki-67 immunostaining (c) in the BVE–PTC tumor transplants. No SA-beta-Gal staining (b) and strong Ki-67 immunostaining (d) in a primary BVE–PTC tumor. (**C**) Increased release of cytokines and chemokines in the fluid of BVE–PTC transplants. Cytokine and chemokine levels were assayed in the fluid of cysts from two BVE–PTC transplants and compared with those in the 48-h culture medium from a BVE–PTC cell line. The value from culture medium alone was subtracted and data are expressed as mean ± s.e.m. of triplicate wells. Only cytokines/chemokines with significant difference are shown ($P < 0.05$). (**D**) Decreased level of cytokines and chemokines in the fluid of cysts from BVE–PTC transplants. Only cytokines/chemokines with significant difference are shown.

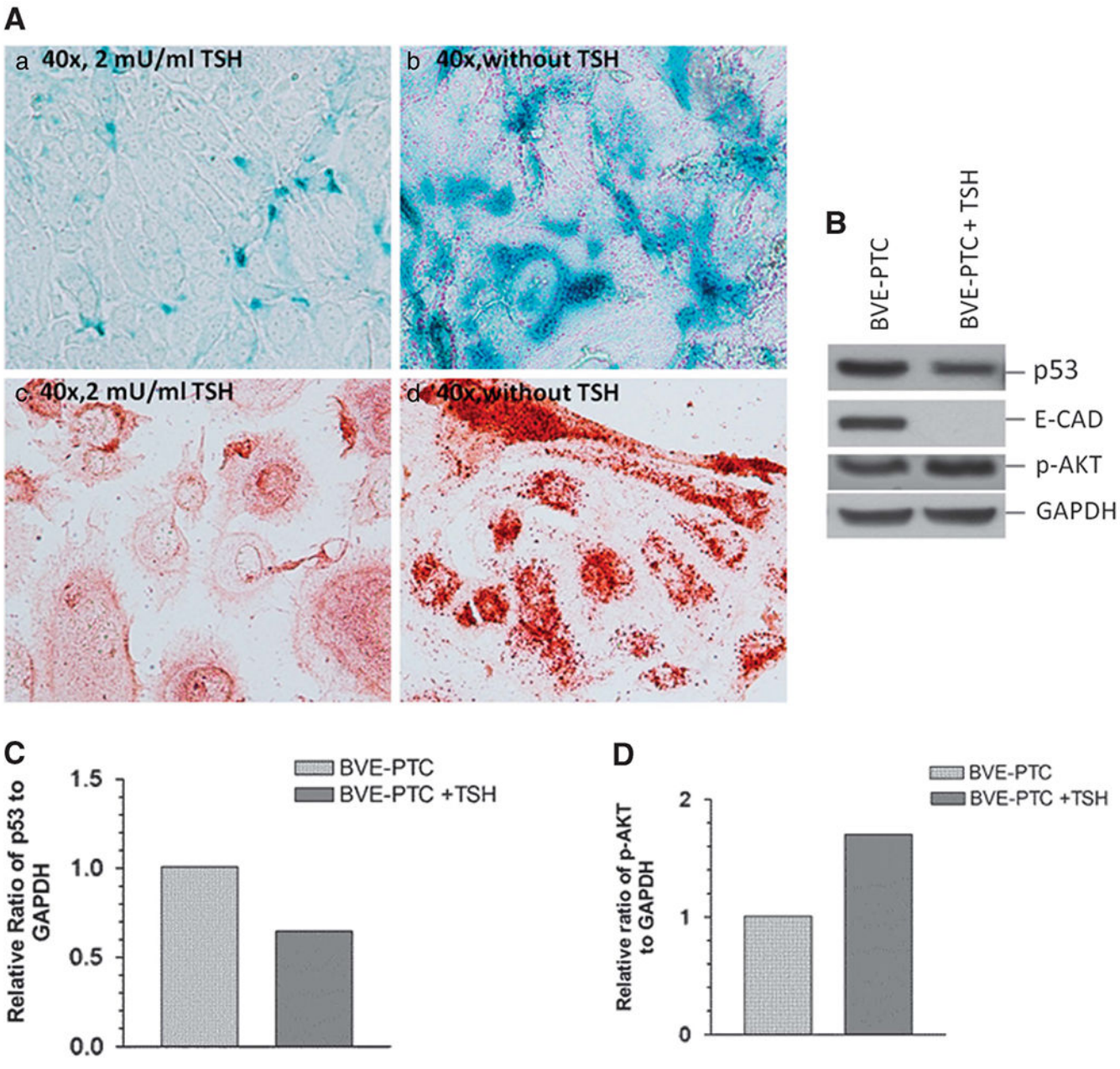

Figure 3.

Inhibition of *Braf*^{V600E}-induced senescence by TSH in BVE–PTC cells. (A) Primary BVE–PTC cells were cultured in the presence of 2 mU/ml of bovine TSH for 2 months and stained for SA-beta-Gal activity (a) and p53 expression (c). Without bovine TSH in the culture, primary BVE–PTC cells could not replicate and was under senescence with strong SA-beta-Gal staining (b) and p53 immunostaining (d). (**B**) Western blot analysis of p53, p-AKT and E-Cadherin expression in a BVE–PTC cell line cultured for 72 h in the presence or absence of 10 mU/ml of bovine TSH. TSH can downregulate both p53 and E-Cadherin expression and increase p-AKT expression. (**C**) Quantification of p53 expression from the western blot

was performed using ImageJ software. (**D**) Quantification of p-AKT expression from the western blot using ImageJ software.

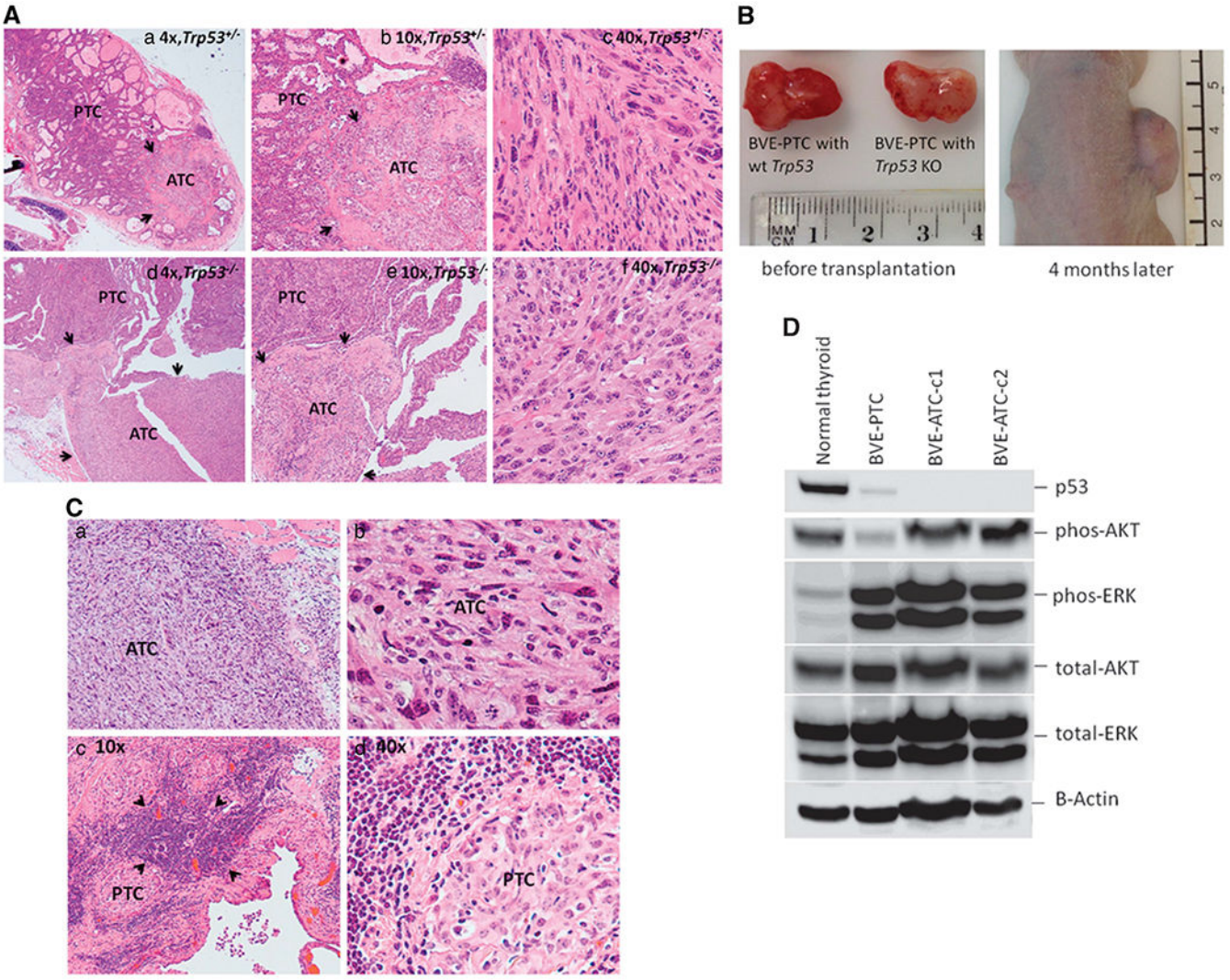

Figure 4.

Trp53 knockout leads to ATC transformation and loss of $Braf^{V600E}$-induced senescence. (**A**) Transformation of PTC to ATC from a 5-month-old TPO–$Braf^{V600E}$–$Trp53^{+/-}$ mouse (heterozygous *Trp53* knockout, a, b, c) and a 3-month-old TPO–$Braf^{V600E}$–$Trp53^{-/-}$ mouse (homozygous *Trp53* knockout, d, e, f). ATC tumors (indicated by arrows) can be seen together with PTC. ATC tumors are larger from TPO–$Braf^{V600E}$–$Trp53^{-/-}$ mice (d, e, f) than from TPO–$Braf^{V600E}$–$Trp53^{+/-}$ mice (a, b, c), and composed of highly pleomorphic giant cells and spindle cells with large, bizarre nuclei containing prominent nucleoli and mitotic figures (c and f). The papillary architecture is replaced by undifferentiated architecture. (**B**) Loss of tumor regression as a result of *Trp53* knockout. Thyroid tumors were removed from 4-month-old TPO–$Braf^{V600E}$ (with wild-type *Trp53*) mice and TPO–$Braf^{V600E}$–$Trp53^{-/-}$ (with *Trp53* knockout) mice. They were transplanted to nude mice and observed for 4 months. Regression of tumor transplant from a TPO–$Braf^{V600E}$ mouse (left) and continued tumor growth from a TPO–$Braf^{V600E}$–$Trp53^{-/-}$ mouse (right) are shown. (**C**) Histology of BVE–PTC tumor transplants. PTC architecture from tumor transplants with $Trp53^{-/-}$ is completely replaced by undifferentiated cellular structure with many giant and

spindle cells characteristic of ATC. Lymphocyte infiltration is not present (a and b). BVE–PTC tumor transplants with *Trp53*$^{+/+}$ are surrounded by heavy lymphocyte infiltration as indicated by arrows and are localized (c and d). (**D**) Western blot analysis of p53, p-ERK and p-AKT expression among normal thyroid, BVE–PTC, BVE–ATC-c1 and BVE–ATC-c2 cell lines. p-AKT expression is significantly increased in BVE–ATC-c1 and BVE–ATC-c2 cell lines as a result of *Trp53* knockout.

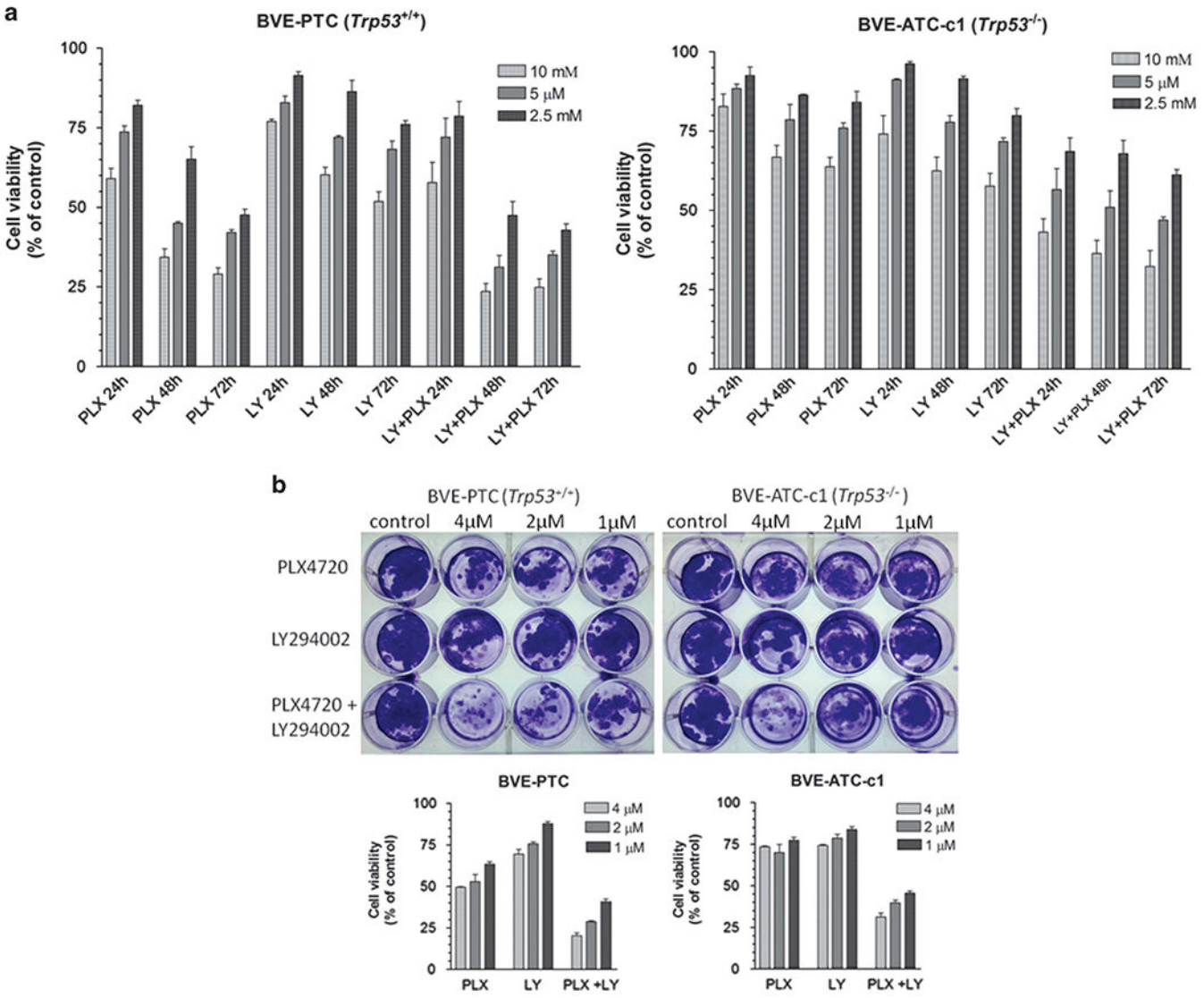

Figure 5.

Effect of simultaneous inhibition of both MAPK and PI3K/AKT pathways against ATC cells. (**A**) Cell proliferation of BVE–PTC and BVE–ATC-c1 cell lines. The cells were plated into 96-well plates (1×10^3 cells/well) and treated with PI3K inhibitor LY294002 or $Braf^{V600E}$ inhibitor PLX4720 alone or in combination for up to 72 h. Cell proliferation was determined by a non-radioactive MTS assay kit. Cells treated with 0.1% dimethyl sulfoxide (DMSO) only were served as a vehicle control. Data are expressed as percentage of the vehicle control (100%) in mean ± s.e.m. of triplicate wells. (**B**) Colony formation assay. Cells were plated into 12-well plates (5×10^2 cells/well) and cultured in the presence of different concentrations of PLX4720, LY294002 or both for 14 days to determine long-term effects of PLX4720 and LY294002. Cells were then stained with 0.5% crystal violet dye (in methanol:de-ionized water, 1:5) for 10 min. After three washes with de-ionized water, the crystal violet dye was released from cells by incubation with 1% sodium dodecyl sulfate

(SDS) for 2 h before optical density $(OD)_{570\ nm}$ measurement. Data are expressed as percentage of the vehicle control.